Hindawi
Advances in Civil Engineering
Volume 2022, Article ID 8141103, 11 pages
https://doi.org/10.1155/2022/8141103

Research Article

Path Attenuation and Source Characteristics during the 2019 Sichuan Changning Earthquake Sequence in China

Zhijun Jiang[1,2], **Lei Zhang**[1,2] **and Qi Zhang**[3]

[1]*Key Laboratory of Earthquake Engineering and Engineering Vibration, Institute of Engineering Mechanics, China Earthquake Administration, Key Laboratory of Earthquake Disaster Mitigation, Ministry of Emergency Management, Harbin 150080, China*
[2]*College of Architectural Science and Engineering, Yangzhou University, Yangzhou 225127, China*
[3]*School of Civil Engineering and Architecture, China Three Gorges University, Yichang 443002, China*

Correspondence should be addressed to Qi Zhang; zhangqi_1988@hotmail.com

Received 12 November 2021; Revised 14 December 2021; Accepted 22 March 2022; Published 26 April 2022

Academic Editor: Qian Chen

To give an insight into the path attenuation and source characteristics of the 2019 Sichuan Changning earthquake sequence, 99 strong-motion recordings at 33 stations were studied. The *S*-wave Fourier amplitude spectra were used to determine the path-attenuation function and key parameters of the seismic source characteristics of this sequence. The results show the following: (1) The geometric spreading effect presents hinged-trilinear characteristics, and the corresponding geometric spreading rates were −0.97, 0.29, and −0.73 with the crossover distances 90 km and 183 km. (2) The quality factor Q is correlated with frequency and expressed as $217 \times f^{0.82}$ for the range from 0.1 to 10.0 Hz. (3) The seismic moment was inversely proportional to the cube of the corner frequency, and their product was 2.37×10^{16} N. m/s^3. (4) The stress drop varied from 1.18 to 12.44 MPa. Both the attenuation effect and source parameters of this sequence are significantly different from those of the Lushan and the Wenchuan aftershock sequences in the Sichuan region of China.

1. Introduction

At 22 : 55 : 43 (UCT+8) on June 17, 2019, an earthquake with magnitude M_s 6.0 struck the town of Shuanghe and its surrounding area in Changning County, Sichuan, China. It is the largest earthquake recorded in the southern margin of Sichuan Basin till now, where seismic activity had been frequented in recent years [1–3]. Then, a series of earthquakes occurred after the mainshock. The Changning Shuanghe anticline was developed in its vicinity, with the axis of the anticline in the northwest (NW)–southeast (SE) direction and the NW section bent to SW. The formation on the north wing of the anticline was steep with a dig angle in the range of 57–60° and an inclination to NE. Some small thrust faults have also developed near the anticline [3]. Hu et al. (2019) determined that the focal mechanism of the Changning main earthquake was a thrust-type earthquake, with a strike-slip component, and its strike/dip/slip angles were 309°/68°/41°, respectively [1].

Sichuan, a province of China located in an area vulnerable to intensive seismic activity, has been struck by several devastating earthquakes, such as the Wenchuan Mw 7.9 Earthquake in 2008, Lushan Mw 6.6 Earthquake in 2013, Jinggu Mw 6.1 Earthquake in 2014, and Jiuzhaigou Ms 7.0 Earthquake in 2017 [4–8]. These earthquakes endured extensive losses of life and property. In addition, several earthquakes occurred in the southern margin of Sichuan Basin, such as the Xingwen Ms 5.7 earthquake in 2018 and Changning Ms 6.0 earthquake in 2019 [9, 10]. To gain an in-depth understanding of the ground motion characteristics of earthquakes in southern margin of Sichuan Basin, studying the propagation and source features of these earthquakes is necessary.

The path attenuation of ground motion primarily involves geometric spreading and anelastic attenuation.

Because of the thickness of the crust and the energy dissipation characteristics of the crustal medium [11–15], the geometric spreading rate, crossover distance, quality factor Q, and other parameters have enhanced discreteness. For the geometric spreading effect in the Sichuan region, Ren et al. (2013) [7] and Wang et al. (2017) [8] inversed the Wenchuan aftershock sequence and the Jiuzhaigou main shock with a geometric spreading rate of -1 (the coefficient of the geometric spreading term). Since the strong-motion stations used in their studies have a small source distance and the seismic rays propagate primarily along the upper crust, a simple geometric spreading term is also used to obtain satisfactory results. To reflect the influence of the Moho reflection mechanism on the seismic wave propagation path, Zhang (2016) [16] used the hinged-bilinear form to reflect the geometric spreading effect in the Sichuan area, and the near-field and far-field geometric spreading rates were -1 and -0.5, respectively. Wen et al. (2015) used a hinged-trilinear function to reflect the geometric spreading effect of the ground motion of the Lushan aftershock sequence while studying the source characteristics of the Lushan aftershock sequence [17]. Regarding the anelastic attenuation of ground motion, Ren et al. (2013), Zhang (2016), Wang et al. (2017), and Wen et al. (2015) determined the crustal quality factors of the Wenchuan, Jiuzhaigou, and Lushan aftershock regions using the generalized inversion method [7, 8, 16, 17]. Wang et al. (2008) and Zhang et al. (2007) used two-dimensional tomography and a genetic algorithm to retrieve the quality factors of the Sichuan Basin [18, 19].

In terms of the source characteristics, Yu et al. (2012) determined the source stress drop parameters of the Wenchuan aftershock sequence [20]. Wen et al. (2015) and Wang et al. (2017) inversed the Lushan earthquake aftershock sequence and the Jiuzhaigou main earthquake and found that the stress drop of the Jiuzhaigou earthquake was greater than that of the Lushan aftershock sequence [8, 17]. Zhang (2016) determined the seismic stress drop, seismic moment, corner frequency, and other key parameters in Western China (including Sichuan, Yunnan, and Gansu), as well as the relationship between the seismic moment and corner frequency [16]. In addition, Liu et al. (2010) obtained the spatial distribution characteristics of the stress drop parameters in the Sichuan area using 323 recordings of small earthquakes based on the Brune source model [21].

The average stress drop of Wenchuan earthquake sequence obtained by Zhang (2016) is larger than that of Lushan aftershock sequence obtained by Wen et al. (2015), and the average stress drop from Yu et al. (2012) and Wang et al. (2017) are the same, which are between the results of Zhang (2016) and Wen et al. (2015). The possible reason is that the magnitude of aftershock sequence selected by Wen et al. (2015) is small, resulting in a small average stress drop. In addition, the stress release in the Longmenshan fault zone during Wenchuan earthquake also led to the smaller average stress drop of Lushan aftershock sequence. Compared with Yu et al. (2012), Zhang (2016) selected the earthquakes from the border of Sichuan and Yunnan, in which the stress drop was significantly larger [21], resulting in a significantly larger average stress drop. These results showed that the path attenuation and focal characteristic parameters of earthquakes in the Sichuan region exhibited obvious spatial variability.

The above conclusions were all based primarily on strong-motion data from North Central Sichuan. At present, the studies on the path attenuation and source characteristics of earthquakes in the Southern margin of Sichuan Basin are few. The strong-motion recordings obtained in the Changning earthquake sequence provided a valuable opportunity to study the source characteristics and path-attenuation effect in this area.

In this study, the Fourier spectrum of the Changning earthquake sequence was analyzed. Its seismic source spectrum, geometric spreading effect, and anelastic attenuation mechanism in the frequency domain were observed. The seismic moment, corner frequency, and stress drop of this earthquake sequence were determined based on the Brune seismic source model [22]. These parameters obtained can, in turn, provide a reference to reveal the attenuation law of ground motion parameters of earthquakes in Sichuan.

2. Data and Processing

Abundant strong motion recordings were obtained when the mainshock of Changning earthquake occurred, and the peak ground acceleration recorded by the station 051GXT was the largest. Its east-west, north-south, and vertical components were 573.47 cm/s^2, 393.77 cm/s^2, and 381.36 cm/s^2, respectively. After the main shock, a series of aftershocks occurred and recorded, namely, four earthquakes with Ms 5.0–5.9, six earthquakes with Ms 4.0–4.9, and 52 earthquakes with Ms 3.0–3.9. The most intense aftershock was the earthquake on July 4, 2019, with Ms 5.6.

For this study, to prevent site amplification caused by terrain effect, improve the accuracy of site amplification estimation and the signal-to-noise ratio of strong-motion recordings. Strong-motion recordings were selected by referring to four criteria, which are as follows:

(1) The magnitude should be larger than Ms 4.0 and R should be less than 300 km because the strong-motion instruments at large distance for small earthquake may not be triggered [23].

(2) Stations should be located in free fields to prevent the influence of topographic effect on the site amplification.

(3) All selected events should be recorded by at least two stations. It is because there should be more recordings for each event to ensure that the scattering of the calculated source and path parameters will be at a relatively low level [7].

(4) The peak ground acceleration of selected recordings should be greater than 1 cm/s^2 because the recordings with low PGA will be contaminated by the noise [7].

Finally, 99 strong-motion recordings at 33 strong-motion stations obtained during nine earthquakes (M_s 4.1–6.0) were selected. The hypocenter locations, focal mechanisms, the style of the faulting of earthquakes [24], and the record numbers are listed in Table 1. Figures 1 and 2 show the

Table 1: Parameters of selected earthquakes used in this study.

No.	Date year/month/day/h/min	Depth (km)	Ms	Longitude (°)	Latitude (°)	Style of faulting	Records number
1	2019/06/17/22/55	16	6.0	104.905	28.344	Reverse-oblique	27
2	2019/06/17/23/36	16	5.1	104.805	28.418	Reverse-oblique	18
3	2019/06/18/00/29	10	4.1	104.845	28.340	Strike-slip	3
4	2019/06/18/00/37	10	4.2	104..874	28.386	Reverse	2
5	2019/06/18/05/03	14	4.5	104.857	28.379	Reverse	3
6	2019/06/18/07/34	17	5.3	104.869	28.368	Reverse	15
7	2019/06/22/22/29	10	5.4	104.793	28.424	Reverse	24
8	2019/06/23/08/28	14	4.6	104.833	28.383	Strike-slip	3
9	2019/06/24/09/23	10	4.1	104.800	28.440	Unknown	4

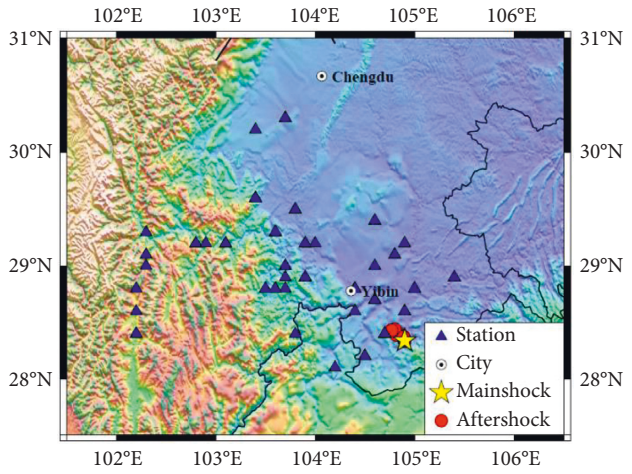

Figure 1: Map showing topography overlapped by the epicenters of the Changning earthquakes (yellow star) and aftershocks (red dot) and the locations of the stations used in this study.

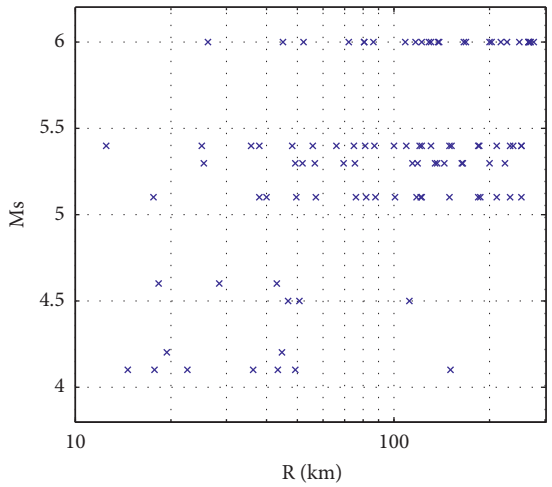

Figure 2: Magnitude of Ms versus distance for all recordings from nine earthquakes.

distribution of the selected earthquake epicenter and station locations and the distance-dependent magnitude of the recordings used in this study, respectively. The horizontal strong-motion seismograms at the station 051YBT for nine earthquakes are shown in Figure 3.

Baseline correction was performed on all recordings, and Butterworth filtering was conducted with a bandwidth ranging from 0.05 to 30 Hz [25]. The 30 Hz low-pass filtering is performed to remove the high-frequency noise, and the high-pass corner frequency was set as 0.05 Hz according to the shape of the Fourier amplitude spectrum at low frequency. In addition, the frequency band studied in this paper is mainly between 0.1 Hz and 20 Hz to ensure that the signal-to-noise ratio of this frequency band is greater than 3. According to the Husid function [26] and the cumulative root-mean-square function [27], the S-wave of the acceleration recordings for the three components were intercepted. The onset of the S-wave arrival time was identified by Husid plot, which shows the buildup of the energy of an accelerogram with time [26]. The end instant of the S-wave was detected using the cumulative root mean square (RMS) function. Specifically, the end instant of the S-wave is defined as the starting point of the decreasing tendency of the cumulative RMS curve along with the time [27]. Figure 4 shows a demonstration of how the onset and the end of the S-wave recorded at 051YBT in Changning mainshock are automatically identified. To remove the truncated error, a cosine-type tapered window was used. Before the onset and after the end of the S-wave, a time series with a duration corresponding to 10% of the S-wave was added to the S-wave part to run the tapering. The magnitude of the Fourier spectrum was calculated from the fast Fourier transform. Then, the Fourier spectrum was smoothed using the method proposed by Konno [28]. Figure 5 shows the calculated and smoothed Fourier spectrum of the NS component at 051YBT in Changning mainshock after filtering. The smoothed Fourier spectra in the two horizontal orthogonal directions were combined within the frequency domain to represent the Fourier spectrum in the horizontal direction [29].

3. Geometric Spreading Effect

Ground motion can be descripted as a convolution of the source, path, and site effects in the time domain. Upon the basic assumption of a point-source earthquake, the observed spectrum of an earthquake can be expressed as a linear multiplication of the following three factors [30]:

$$O_{ij}\left(f, R_{ij}\right) = S_i(f)P\left(f, R_{ij}\right)G_j(f), \quad (1)$$

where O_{ij} is the Fourier spectrum of the observed ground motion of Station j in earthquake i (i refers to the number of

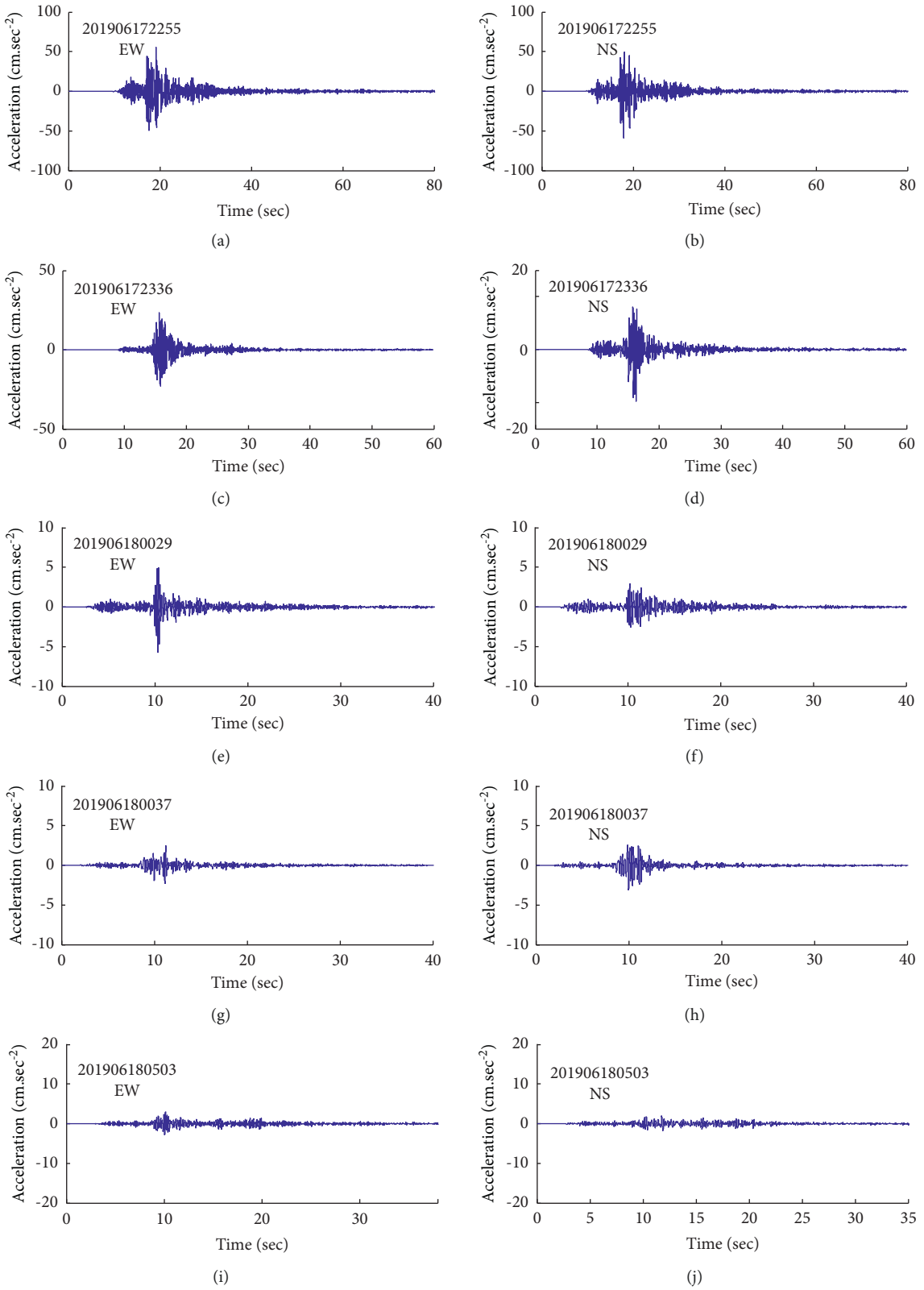

Figure 3: Continued.

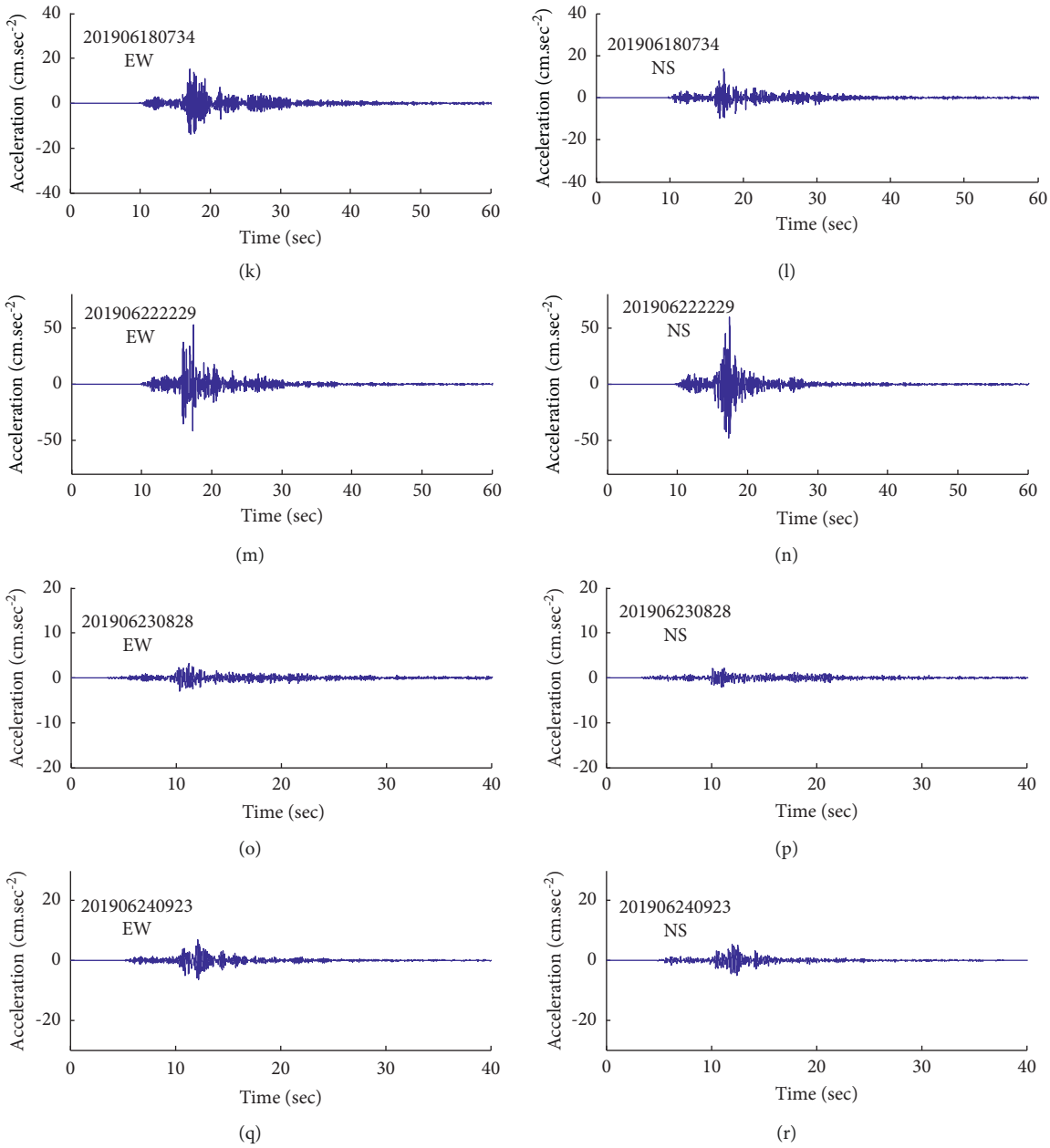

Figure 3: The horizontal strong-motion seismograms for nine earthquakes at the station 051YBT.

the earthquake in Table 1, and the unit of Fourier spectrum is $m{\cdot}s^{-1}$), S_i is the source spectrum of earthquake i, P_{ij} is the path-attenuation function that represents the path effect, R_{ij} is the distance between Station j and earthquake i, and it refers to the source distance in this study, and G_j is the site response of Station j. The distance attenuation term P_{ij} in equation (1) consists of the geometric spreading and anelastic attenuation effects, which can be rewritten as

$$P_{ij}(f) = g\left(R_{ij}\right)\exp\left(\mathrm{d}(f)R_{ij}\right), \tag{2}$$

where $g\ (R_{ij})$ is the geometric spreading function, and the rest is the anelastic attenuation effect is as follows:

$$\mathrm{d}(f) = -\frac{\pi f}{Q_S(f)}\beta_S, \tag{3}$$

where $Q_S(f)$ is the frequency-dependent S-wave quality factor of the crustal medium, and β_S is the shear-wave velocity of the crust. $\beta_S = 3.6$ km/s in this study [31–33]. Substituting equation (2) in equation (1) and applying the logarithm of both sides of the resulting equation yields the following form:

$$\ln\left[O_{ij}(f)\right] - \ln\left[S_i(f)\right] - \ln\left[G_j(f)\right] = \ln\left(P_{ij}(f)\right), \tag{4}$$

$$\ln\left(P_{ij}(f)\right) = \ln\left[g\left(R_{ij}\right)\right] + d(f)R_{ij}. \tag{5}$$

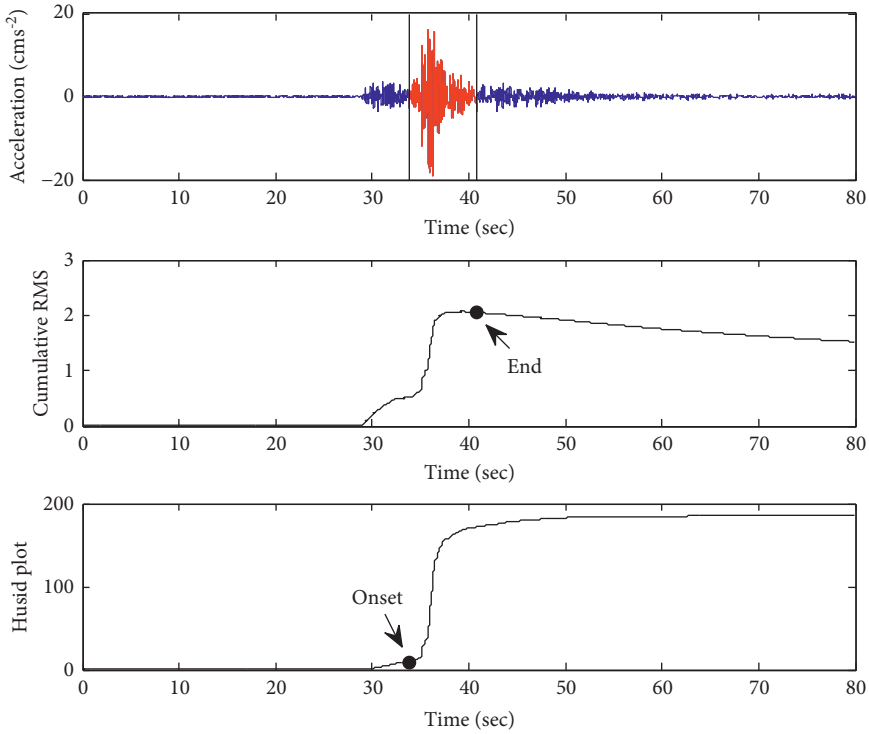

Figure 4: The detection of the S-wave of the NS component at 051YBT in Changning mainshock.

The geometric spreading function $g\ (R_{ij})$ can be expressed in the form of a hinged-trilinear [13], as given in

$$g(R) = \begin{cases} b_1 \ln(R), & R_{ij} \le R_1 \\ b_1 \ln(R_1) + b_2 \ln\left(\dfrac{R}{R_1}\right), & R_1 < R_{ij} \le R_2 \\ b_1 \ln(R_1) + b_2 \ln\left(\dfrac{R_2}{R_1}\right) + b_3 \ln\left(\dfrac{R}{R_2}\right), & R_{ij} > R_2 \end{cases}. \quad (6)$$

The parameters b_1, b_2, b_3, R_1, and R_2 are regression coefficients. R_1 and R_2 are the crossover distances at which the geometric spreading rate changes.

To determine the geometric spreading function as shown in equation (6), the source spectrum, site response, and anelastic attenuation term must be eliminated.

The site response term $G_j(f)$ in equation (4) can be rewritten as follows:

$$G_j(f) = A_j(f)\exp(-\pi\kappa_0 f), \quad (7)$$

where $A_j(f)$ is the site amplification provided by the near-surface soil, and κ_0 represents the attenuation effect of the soil layer near the surface on high-frequency ground motions. The velocity of the shear wave at the sites of the strong-motion stations is typically required to determine the site response, $A_j(f)$. Most stations selected in this study lacked wave velocity data. Thus, $A_j(f)$ was approximated by the horizontal-to-vertical ratio (H/V) of the Fourier spectrum [34]. Anderson and Hough (1984) [35] suggested a way to

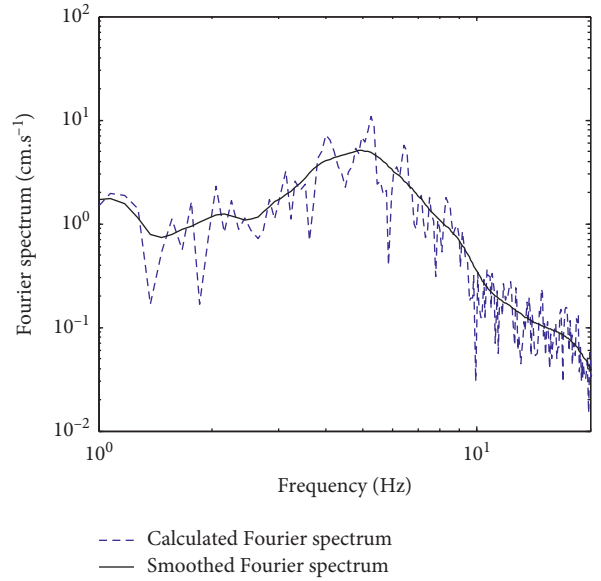

Figure 5: The calculated and smoothed Fourier spectrum of the NS component at 051YBT in Changning mainshock after filtering.

describe the shape of the high-frequency part of the Fourier amplitude spectrum with

$$O_{ij}(f) = O_0 \exp(-\pi\kappa f), \quad (8)$$

where O_0 is the ground motion amplitude determined by the seismic source and path term, and κ is the near-surface attenuation coefficient that can control the frequency-dependent attenuation rate of the amplitude. Equation (7) was

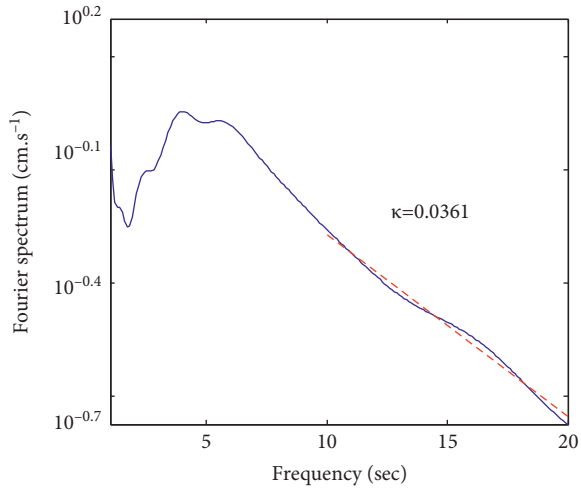

FIGURE 6: Calculation diagram of κ using the vertical component of Fourier spectrum at 051YBT in Changning mainshock.

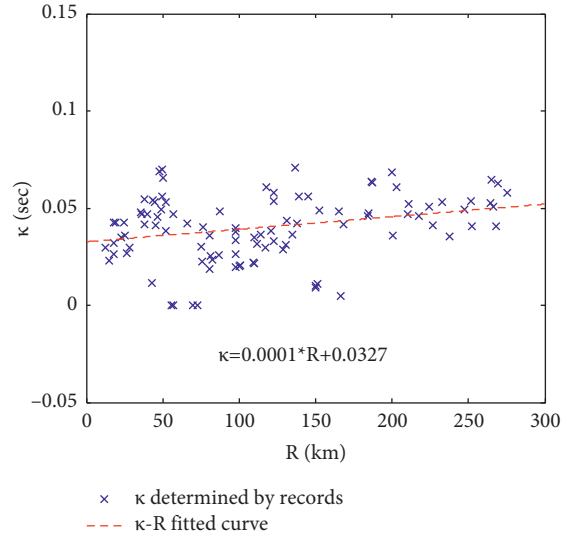

FIGURE 7: Dependency between κ and distance.

fitted using the recordings of each station in a single logarithmic coordinate system to obtain the κ-value of each station site. Take the slope of Fourier spectrum in the range of 10Hz-20 Hz as k. Then, $\kappa = k/(-\pi \times \lg e)$ [35]. Figure 6 gives the calculation diagram of κ using the vertical component of the Fourier spectrum at 051YBT in Changning mainshock. The dependency of κ on the source distance R at each station was then fitted based on a first-order relationship to obtain the coefficient κ_0. Notably, a part of the κ_0-value has already been accounted for in the H/V ratio. Thus, it should be subtracted from the near-surface attenuation term for the horizontal component [34]. Hence, the site response for the horizontal component can be rewritten as follows:

$$G_j(f) = \frac{H}{V}\exp(-\pi\kappa_{0V} f), \tag{9}$$

where κ_{0v} should be determined via the vertical Fourier spectrum of the ground motion. Figure 7 shows the distance-dependent variation of κ with respect to the vertical component of the recordings as contained in this dataset. By fitting the data points, as shown in Figure 7, κ_{0v} can be determined as 0.0327. The average value of H/V from the same station can then be calculated. Based on κ_0v, the site response term $G_j(f)$ can be obtained using equation (8). $G_j(f)$ is then substituted in equation (4) to eliminate the influence of site response and modify the observed ground motion to the corresponding value of the bedrock site.

To determine the source spectrum S_i, the path-attenuation term must be used to modify the Fourier spectrum of the bedrock site to the source position after the effect of the site response is eliminated. Therefore, the path-attenuation term must be determined first. The geometric spreading and anelastic attenuation terms are coupled. Thus, it is difficult to separate them using strong motion data. The geometric attenuation term is generally considered independent of frequency [11, 13, 34, 36], and the effect of anelastic attenuation can be ignored in the near-field ($R < 100$ km) [36]. Consequently, the source spectrum of each earthquake was initially determined using the observed ground motion with a distance shorter than 100 km. According to the theory of seismic wave propagation, the source spectrum can be derived from the correction of the observed value of the Fourier spectrum at the bedrock site using the geometric spreading effect function (R^{-1}) [34]. Accordingly, the corrected values of the Fourier spectrum from the same earthquake were averaged to obtain the approximate value of the first-order estimate of the source spectrum S_i of this earthquake [36].

The distance attenuation $P_{ij}(f)$ can be obtained by substituting S_i and G_j in equation (4). When the frequency is 0.3 Hz, the dependence of $P_{ij}(f)$ on R is shown in Figure 8. As observed from Figure 8, $P_{ij}(f)$ rapidly decreases as R increases; however, $P_{ij}(f)$ decreases at a decelerated rate as R increases. When R is greater than the threshold, the decrease rate of $P_{ij}(f)$ increases again, clearly indicating the effect of the reflection mechanism of the Moho surface.

To determine the parameters b_1, b_2, b_3, R_1, and R_2, the value range of each coefficient was set up, and the optimal solution of the path effect function nearest to the data point trend was identified using the grid search method. The value ranges of b_1, b_2, b_3, R_1, R_2, and d for grid search are -0.8~-1.3, -0.5~0.5, -0.4~-1, 50~100, 100~200, and -0.01~0, respectively. Based on the grid search method, the mean values of b_1, b_2, b_3, R_1, and R_2 are -0.97, 0.29, -0.73, 90 km, and 183 km, respectively.

The curve of the obtained path-attenuation term ($f = 0.3$ Hz) is plotted in Figure 8. It can be observed that the data points are evenly distributed on both sides of the fitted curve. Meanwhile, the path-attenuation terms of the Lushan and Wenchuan aftershocks obtained by [7, 17] are also provided. These terms were obtained by substituting the geometric attenuation function and Q-value in [7, 17] in equations (2) and (3). Given that Wen et al. (2015) and Ren et al. (2013) represented the path-attenuation characteristics of the Lushan and the Wenchuan aftershock sequences, respectively, the difference between them and the results in

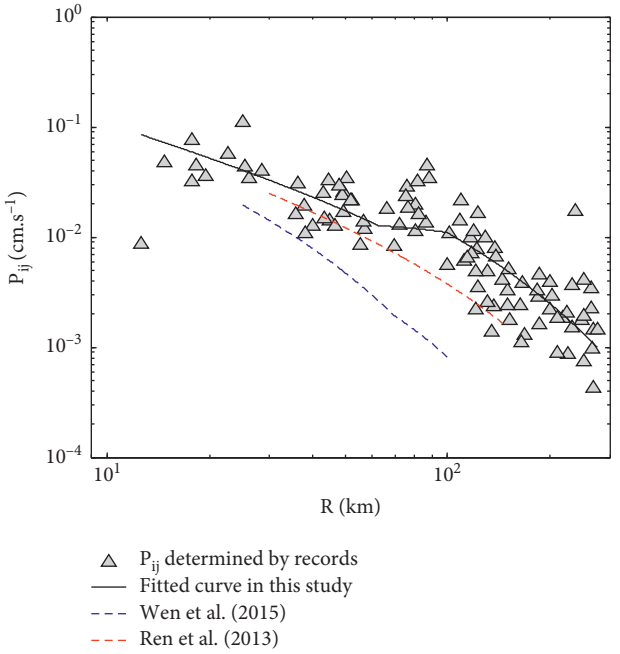

Figure 8: Distribution of P_{ij}(f) versus hypocentral distance.

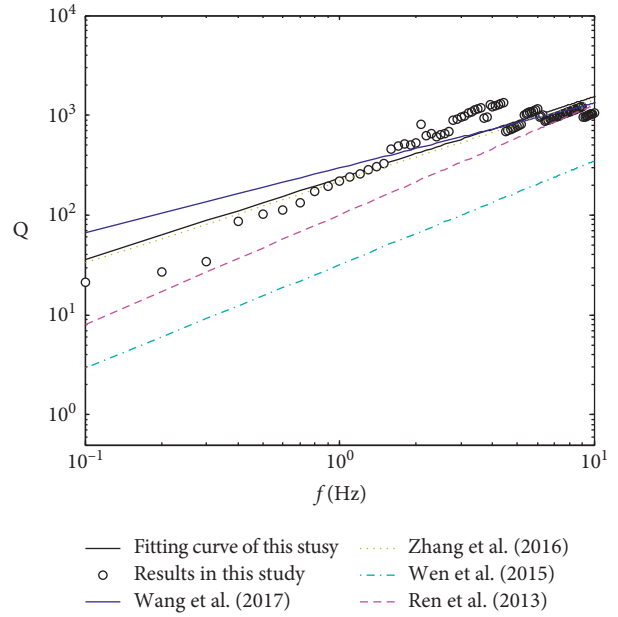

Figure 9: Quality factor Q for Changning earthquake region.

this study showed that the path-attenuation effect of the Changning earthquake sequence was different from those of the Lushan and the Wenchuan aftershock sequences.

4. Quality Factor Q

The coefficient $d(f)$ was determined by the grid search method, and the quality factor Q(f) of the S-wave can be determined using equation (3). The variation trend of the quality factor Q(f) with frequency is shown in Figure 9. The relationship between Q and f was fitted in the form of $Q(f) = Q_0 f^n$ and $Q(f) = 217f^{0.82}$. Meanwhile, other research results in Sichuan are presented. Notably, the Q-value results in this study are larger than those of [7, 17] but close to the results of [18, 19]. It shows that the Q-value in the Changning earthquake area is larger than that in the Lushan and Wenchuan aftershock areas but close to the average level of the Q-value in the Sichuan area.

The Q-value of the quality factor in this study was higher than that of [7, 17]. There are two reasons that can interpret it. (1) Compared with the strong motion recordings selected by [7, 17], the hypocenter distance of this dataset was larger, the seismic rays, which arrived at the far-field station, passed through the deeper crustal medium, and the quality factor Q of the deep-crustal medium was larger. (2) The quality factor of the crustal medium was correlated with the thickness of the crust. It is generally believed that the quality factor is smaller when the crust thickness is larger [34]. The Changning earthquake sequence occurred in the southern margin of the Sichuan Basin and the areas studied by [7, 17] were located in the North Central Sichuan. The crustal thickness in Sichuan increased gradually from south to north [37]. This trend is consistent with the spatial distribution trend of the Q-value obtained by [7, 17].

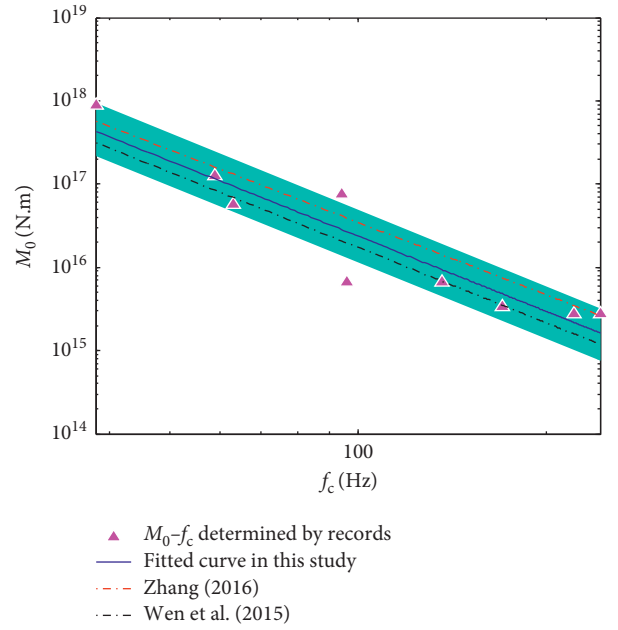

Figure 10: Seismic moment M_0 versus the corner frequency f_c.

5. Seismic Source Spectrum

The path-attenuation term $P_{ij}(f)$ (both the geometric and anelastic attenuation terms) was derived from a previous study. If G_j and $P_{ij}(f)$ are known, the source spectrum can be determined more accurately according to equation (4) using the full dataset as the influence of the quality factor Q was considered. The source displacement spectrum $S(f)$ (ratio of $(2\pi)^2$ to the source acceleration spectra) can be expressed as follows:

Table 2: Source parameters obtained in this study.

No. of earthquakes	1	2	3	4	5	6	7	8	9
$\Delta\sigma$ (MPa)	9.55	5.17	3.36	3.29	1.18	2.84	12.45	5.95	7.90
$f_{c/}$ (Hz)	0.38	0.59	1.36	1.7	0.96	0.63	0.94	2.22	2.44
M_0/N.m($\times 10^{17}$)	8.81	1.27	0.068	0.034	0.068	0.58	0.76	0.028	0.028

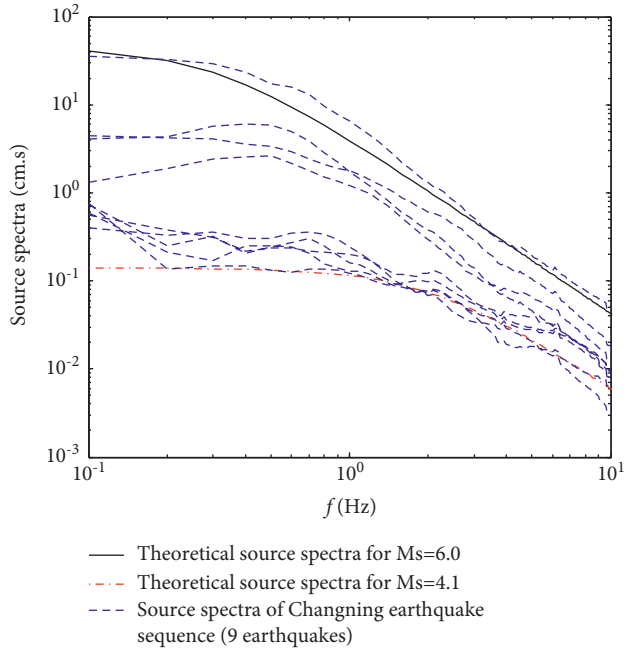

Figure 11: Seismic source displacement spectra versus the theory model of the Changning seismic sequence.

$$S(f) = \frac{\Re_{\Theta\Phi} VF}{4\pi\rho\beta_s{}^3 R_0} \frac{M_{0i}}{1 + f/f_{ci}{}^2}, \quad (10)$$

where $\Re_{\Theta\Phi}$ is the radiation pattern, which is usually equal to $\sqrt{2/5}$ [16]. F reflects the free-surface effect of the shear-wave, with a value set to 2.0. V is the distribution coefficient that considers the S-wave energy along two orthogonal directions whose values are typically set to 0.7. Additionally, ρ is the rock mass density of the seismic source, whose value was set to 2.8 g/cm^3 in this study. β_S is the average shear-wave velocity of the rock in the seismic source area, with an approximate value of 3.6 km/s. R_0 is the reference distance of the seismic source, with a value of 1 km. M_{0i} is the seismic moment of earthquake i, and f_{ci} is the corner frequency of the source spectrum of earthquake i.

Using the seismic source displacement spectrum, the seismic moment M_{0i} and corner frequency f_{ci} of each earthquake can be determined from the least-squares fitting using the interval search algorithm. The search interval of magnitude is M - 0.5~M + 0.5, and the search interval of f_c is 0.02~5 Hz. When the frequency is between 0.1 and 10 Hz, the solution that can minimize the difference between the theoretical source displacement spectrum and the observed result is the optimal solution.

Figure 10 presents the relationship between the determined seismic moment M_0 and corner frequency f_c for the Changning sequence with a 68.3% confidence interval. The relationship between M_0 and the corner frequency f_c shows an obvious inverse relationship, and the relationship between M_0 and f_c is $M_0 f_c^3 = 2.37 \times 10^{16}$ N·m/s^3. This relationship indicates that the seismic source features of the Changning seismic sequence show self-similarity. The results of Zhang (2016) [16] and Wen et al. (2015) [17] are also presented. The results of [16, 17] differ from those obtained in this study, however, they are included in the 68.3% confidence interval. The comparison results show that the relationship between M_0 and f_c for the Changning earthquake sequence is slightly different from those of the Wenchuan earthquake sequence and the Lushan aftershock sequence.

The stress drop parameter $\Delta\sigma$ can be derived from equation (11) given the values of *M0* and *fc*, and the resulting $\Delta\sigma$ and f_c of the Changning earthquake sequence are listed in Table 2. Using equation (11), the mean stress drop value of 4.68 MPa can be determined, which is close to the mean stress drop value of 4.89 MPa for global intraplate earthquakes [38]. Wen et al. (2015) and Yu (2012) obtained the mean stress drop values of 3.14 MPa and 3.8 MPa for the Lushan and Wenchuan aftershock sequences, respectively. These values are lower than those of the Changning earthquake sequence.

$$\Delta\sigma = \frac{7M_0}{16}\left(\frac{2\pi f_c}{2.34\beta_s}\right)^3. \quad (11)$$

Figure 11 presents the displacement spectra of the source of the Changning earthquake sequence with magnitudes derived in this study in the range of 4.1<Ms<6.0. The calculated Brune theoretical displacement spectra for two earthquakes with magnitudes Ms 4.1 and Ms 6.0, with a $\Delta\sigma$ of 4.68 MPa, are also provided. It can be observed that, even though the stress decrease ($\Delta\sigma$) associated with the Changning earthquake sequence was relatively discrete, the displacement spectra of the seismic sources matched the theoretical model, as well as the theoretical values, thus indicating that the seismic sources of this earthquake sequence conform to the Brune (1970) point-source model.

6. Conclusions

In this study, the path-attenuation effect term and seismic source characteristic parameters of the Changning earthquake sequence were derived based on the analyses of the S-wave Fourier amplitude spectra of strong-motion recordings obtained from 33 strong-motion stations in nine

earthquakes of the 2019 Changning earthquake sequence. The main conclusions were as follows:

(1) The path-attenuation effect of the Changning earthquake sequence matched the mechanism associated with the Moho effect, and the attenuation trend of the ground motion with the propagation path was significantly different from that of the aftershock sequences of Lushan and Wenchuan.

(2) The geometric spreading term of the Changning earthquake sequence exhibited hinged-trilinear characteristics, with average geometric spreading rates of -0.97, 0.29, and -0.73 in the three segments and average crossover distances of 90 km and 183 km. The quality factor Q was correlated with frequency, and the relationship between the two was $Q(f) = 217 \times f^{0.82}$ in the frequency band of 0.1–10 Hz. The Q-value was larger than that of the aftershock areas of Lushan and Wenchuan but close to the average Q-value in Sichuan.

(3) The seismic moment of the Changning earthquake sequence varied from 2.75×10^{15} N·m to 8.75×10^{17} N·m, and the corner frequency varied from 0.38 Hz to 2.36 Hz. The seismic moment was inversely proportional to the cube of the corner frequency, and the product was 2.37×10^{16}N.m/s^3. It indicated that the seismic source features of the Changning seismic sequence show self-similarity. The stress drop $\Delta\sigma$ ranged between 1.18 and 12.44 MPa, with an average value of 4.68 MPa. The source characteristics were different from those of the Wenchuan earthquake sequence and the Lushan aftershock sequence.

Data Availability

Data for this study were provided by China Strong Motion Network Centre at Institute of Engineering Mechanics, China Earthquake Administration.

Conflicts of Interest

The authors declare that there are no conflicts of interest regarding the publication of this paper.

Acknowledgments

The authors thank the Scientific Research Fund of the Institute of Engineering Mechanics, China Earthquake Administration (Grant nos. 2018D11 and 2020D13), the Science and Technology Research Project of Education Department of Hubei Province (Grant no. Q20191210), and the Ministry of Housing and Urban-Rural Development of China Research Project (No.2017-K9-010). The authors also thank China Strong Motion Network Centre at Institute of Engineering Mechanics, China Earthquake Administration, for providing the data for this study.

References

[1] X. H. Hu, S. Z. Sheng, and Y. G. Wan, "Study on focal mechanism and post-seismic tectonic stress field of the Changning," *Progress In Geophysics*, vol. 5, 2020.

[2] X. Lei, Z. Wang, and J. Su, "The december 2018 ML 5.7 and january 2019 ML 5.3 earthquakes in south Sichuan Basin induced by shale gas hydraulic fracturing," *Seismological Research Letters*, vol. 90, no. 3, pp. 1099–1110, 2019.

[3] P. Wu, J. R. Su, and C. M. Huang, "Characteristic of shear-wave splitting in the Yibin area, Sichuan province," *Earthquake Research in China*, vol. 33, no. 3, pp. 414–423, 2017.

[4] J. Hu, W. Zhang, L. Xie, Q. Zhang, and Z. Jiang, "Strong motion characteristics of the M w 6.6 Lushan earthquake, Sichuan, China - an insight into the spatial difference of a typical thrust fault earthquake," *Earthquake Engineering and Engineering Vibration*, vol. 14, no. 2, pp. 203–216, 2015.

[5] J. J. Hu, Q. Zhang, Z. J. Jiang, L. L. Xie, and B. F. Zhou, "Characteristics of strong ground motions in the 2014 M s 6.5 Ludian earthquake, Yunnan, China," *Journal of Seismology*, vol. 20, no. 1, pp. 361–373, 2016.

[6] Y. Ren, H. Wang, P. Xu et al., "Strong-motion observations of the 2017 Ms 7.0 Jiuzhaigou earthquake: comparison with the 2013 Ms 7.0 lushan earthquake," *Seismological Research Letters*, vol. 89, no. 4, pp. 1354–1365, 2018.

[7] Y. Ren, R. Wen, H. Yamanaka, and T. Kashima, "Site effects by generalized inversion technique using strong motion recordings of the 2008 Wenchuan earthquake," *Earthquake Engineering and Engineering Vibration*, vol. 12, no. 2, pp. 165–184, 2013.

[8] H. W. Wang, Y. F. Ren, and R. Z. Wen, "Source spectra of the 8 August 2017 Jiuzhaigou Ms7.0 earthquake and the quality factor of the epicenter area," *Chinese Journal of Geophysics*, vol. 60, no. 10, pp. 4117–4123, 2017.

[9] X. Lei, Z. W. Wang, Z. Wang, and J. Su, "Possible link between long-term and short-term water injections and earthquakes in salt mine and shale gas site in Changning, south Sichuan Basin, China," *Earth and Planetary Physics*, vol. 3, no. 6, pp. 510–525, 2019.

[10] X. Lei, J. Su, and Z. Wang, "Growing seismicity in the Sichuan Basin and its association with industrial activities," *Science China Earth Sciences*, vol. 63, no. 11, pp. 1633–1660, 2020.

[11] T. I. Allen and G. M. Atkinson, "Comparison of earthquake source spectra and attenuation in eastern North America and southeastern Australia," *Bulletin of the Seismological Society of America*, vol. 97, no. 4, pp. 1350–1354, 2007.

[12] T. I. Allen, P. R. Cummins, T. Dhu, and J. F. Schneider, "Attenuation of ground-motion spectral amplitudes in southeastern Australia," *Bulletin of the Seismological Society of America*, vol. 97, no. 4, pp. 1279–1292, 2007.

[13] G. M. Atkinson and R. F. Mereu, "The shape of ground motion attenuation curves in southeastern Canada," *Bulletin of the Seismological Society of America*, vol. 82, no. 5, pp. 2014–2031, 1992.

[14] A. Zandieh and S. Pezeshk, "Investigation of geometrical spreading and quality factor functions in the new madrid seismic zone," *Bulletin of the Seismological Society of America*, vol. 100, no. 5A, pp. 2185–2195, 2010.

[15] A. Zandieh, S. Pezeshk, and K. W. Campbell, "An equivalent point-source stochastic simulation of the NGA-west2 ground-motion prediction equations," *Bulletin of the Seismological Society of America*, vol. 108, no. 2, pp. 815–835, 2018.

[16] Q. Zhang, "Study on regional differentiation of ground motion attenuation relationship," Doctorate Dissertation,

Institute of Engineering Mechanics China Earthquake Administration, Harbin, 2016.
[17] R. Z. Wen, H. W. Wang, and Y. F. Ren, "Estimation of source parameters and quality factor based on generalized inversion method in Lushan earthquake," *Journal of Harbin Institute of Technology*, vol. 47, no. 4, pp. 58–63, 2015.
[18] S. Y. Wang, S. P. Pei, and Z. H. Xu, "Crustal S-wave Q estimated from ML amplitude I:attenuation in different tectonic regions of China," *Chinese Journal of Geophysics*, vol. 50, no. 6, pp. 1740–1747, 2007.
[19] Y. J. Zhang, H. Z. Qiao, and W. Z. Cheng, "Attenuaiton characteristics of the media in Sichuan Basin region," *Journal of Seismological Research*, vol. 30, no. 1, pp. 43–48, 2007.
[20] T. Yu and X. J. Li, "Inversion of strong motion data for source parameters of Wenchuan afershocks, attenuation function and average site effect," *Acta Seismologica Sinica (Chinese edition)*, vol. 34, no. 5, pp. 621–632, 2012.
[21] L. F. Liu, Y. J. Su, and J. Liu, "Study on temporal and spatial features of stress drop for low-to-moderate earthquake in sichuan and yunnan region," *Journal of Seismological Research*, vol. 33, no. 3, pp. 314–319, 2010.
[22] J. N. Brune, "Tectonic stress and the spectra of seismic shear waves from earthquakes," *Journal of Geophysical Research*, vol. 75, no. 26, pp. 4997–5009, 1970.
[23] D. M. Boore, J. P. Stewart, E. Seyan, and G. M. Atkinson, "NGA-West2 equations for predicting response spectral accelerations for shallow crustal earthquakes," PEER Report, 2013.
[24] G. X. Yi, F. Long, and M. J. Liang, "Focal mechanism solutions and seismogenic structure of the 17 June 2019 Ms6.0 Sichuan Changning earthquake sequence," *Chinese Journal of Geophysis*, vol. 62, no. 9, pp. 3432–3447, 2019.
[25] H. Wang and R. Wen, "Attenuation and basin amplification revealed by the dense ground motions of the 12 july 2020 Ms 5.1 tangshan, China, earthquake," *Seismological Research Letters*, vol. 92, no. 4, pp. 2109–2121, 2021.
[26] R. Husid, "Gravity effects on the earthquakes response of yielding structures," Ph. D. thesis, California Institute of Technology, Los Angeles, 1967.
[27] M. W. McCann and H. C. Shah, "Determining strong-motion duration of earthquakes," *Bulletin of the Seismological Society of America*, vol. 69, no. 4, pp. 1253–1265, 1979.
[28] K. Konno and T. Ohmachi, "Ground-motion characteristics estimated from spectral ratio between horizontal and vertical components of microtremor," *Bulletin of the Seismological Society of America*, vol. 88, no. 1, pp. 228–241, 1998.
[29] S. Drouet, S. Chevrot, F. Cotton, and A. Souriau, "Simultaneous inversion of source spectra, attenuation parameters, and site responses: application to the data of the French accelerometric Network," *Bulletin of the Seismological Society of America*, vol. 98, no. 1, pp. 198–219, 2008.
[30] D. M. Boore, "Simulation of ground motion using the stochastic method," *Pure and Applied Geophysics*, vol. 160, no. 3, pp. 635–676, 2003.
[31] X. W. Bao, X. X. Sun, M. J. Xu et al., "Two crustal low-velocity channels beneath SE Tibet revealed by joint inversion of Rayleigh wave dispersion and receiver functions," *Earth and Planetary Science Letters*, vol. 415, pp. pp16–24, 2015.
[32] G. Laske, G. Masters, Z. Ma, and M. Pasyanos, "Update on CRUST1.0 - a 1-degree global model of earth's crust," in *Proceedings of the EGU General Assembly Conference*, Vienna, Austria, April, 2013.
[33] Y. Luo, L. F. Zhao, Z. X. Ge, X. B. . Xie, and Z. X. Yao, "Crustal Lg-wave attenuation in Southeast Asia and its implications for regional tectonic evolution," *Geophysical Journal International*, vol. 226, pp. 1873–1884, 2021.
[34] A. Meghdadi and J. Shoja-Taheri, "Ground-motion attenuation and source spectral shape for earthquakes in eastern Iran," *Bulletin of the Seismological Society of America*, vol. 104, no. 2, pp. 624–633, 2014.
[35] J. G. Anderson and S. E. Hough, "A model for the shape of the fourier amplitude spectrum of acceleration at high frequencies," *Bulletin of the Seismological Society of America*, vol. 74, pp. 1969–1993, 1984.
[36] G. M. Atkinson, "Empirical attenuation of ground-motion spectral amplitudes in southeastern Canada and the northeastern United States," *Bulletin of the Seismological Society of America*, vol. 94, no. 3, pp. 1079–1095, 2004.
[37] L. Dong, X. Z. Shen, and Y. P. Qian, "Study on velocity and density contrasts across the Moho in the southeastern margin of the Tibetan Plateau," *Chinese Journal of Geophysics*, vol. 63, no. 3, pp. 915–927, 2020.
[38] B. P. Allmann and P. M. Shearer, "Global variations of stress drop for moderate to large earthquakes," *Journal of Geophysical Research: Solid Earth*, vol. 114, no. B1, 2009.